

# Optical and Visual Performance of PWM Controlled InGaN and InGaAlP LEDs for Automotive Lighting Applications

Miroslav Slouka<sup>1</sup>, Ladislav Stanke<sup>2</sup>, Martin Kutáč<sup>3</sup>, and Jan Látal<sup>4</sup>, *Member, IEEE*

**Abstract**—This research investigates the light quality and thermal management of InGaN and InGaAlP Light Emitting Diodes (LEDs) under various light regulation methods. We compare Continuous Wave (CW) and Pulse-Width Modulation (PWM) modes, examining their impacts on luminous flux, temperature, total color shift, and angular color shift. Our findings reveal that the CW mode offers higher luminous flux and reduced temperatures, while the PWM mode ensures enhanced color stability across different currents and viewing angles, especially for white LEDs; however, this stability does not extend to other LED types. From both optical and visual performance perspectives, the study emphasizes optimizing the driving current to meet regulatory requirements and ensure consistent color perception. These insights are crucial for automotive lighting design, contributing to improved regulatory compliance and aesthetic quality.

**Index Terms**—Automotive exterior lighting, colorimetry, color shift, LED, lighting technology, photometry, PWM.

## I. INTRODUCTION

AS THE automotive lighting landscape advances, transitioning from traditional incandescent bulbs and halogen lamps to more efficient Light Emitting Diodes (LEDs) signifies a significant step toward innovation and energy conservation [1]. This shift involves a change in the light source and reflects the pursuit of enhanced efficiency, superior light quality, and refined thermal management [2]. These aspects are influenced by the method of light regulation, which is crucial for determining the operational characteristics of illumination devices. In automotive applications, brightness control methods

include Continuous Wave (CW) and Pulse-Width Modulation (PWM) [3]. This article scrutinizes the usability of PWM in various semiconductor lighting applications [4].

For non-luminophore LEDs, the color change is different depending on the material and structure of the chip. In InGaN LEDs (blue and green), the color shift with increasing current is primarily caused by the band-filling effect. As electrons occupy higher energy levels, the transition energy increases, leading to a blue shift [5], [6]. This effect is dominant at higher currents. With increasing temperature, a red shift occurs, which is attributed to the thermal narrowing of the bandgap. However, this shift is relatively small compared to other types of LED [7]. In contrast, AlInGaP LEDs (red) show a more significant red shift with increasing temperature due to this thermal band gap narrowing [8]. Unlike InGaN LEDs, the current has a much smaller influence on the color shift in AlInGaP LEDs, where the temperature remains the dominant factor [5], [6]. Current is a significant factor in InGaN LEDs, and temperature plays a crucial role in AlInGaP LEDs. The quantum-confined Stark effect, caused by internal polarization fields, can also contribute to the redshift. However, this effect is independent of temperature and is more pronounced in larger quantum wells [9].

Phosphor-converted (PC) LEDs are used to realize a white color. The phosphor is, therefore, another element that generalizes the color change. This change is mainly influenced by its concentration. Higher phosphor concentrations convert blue light into yellow, producing white light but also leading to increased backscattering and heat, which can reduce efficiency, especially in constant current operation [10], [11]. Phosphor configurations in LEDs typically follow two approaches: a conformal structure, where the phosphor layer is coated on the LED die, or a dispensing structure, where the phosphor forms a dome around the LED. To achieve a smaller Angular Correlated Color Temperature Deviation (ACCTD), allowing the light rays emitted from the blue die to travel the same path within the phosphor volume [12] is imperative. ACCTD can be improved using screen-printed multilayer phosphor-in-glass (PiG) designs, significantly reducing ACCTD values. Cone-shaped PiG structures enhance light mixing and minimize color variations [13]. In addition to the mechanisms mentioned above for the occurrence of non-uniformities related mainly to the driving of LED and omnidirectional observation, there are other material phenomena such as phosphor degradation [14] that might cause a blue, green, yellow, or red shift as well. These

Received 8 August 2024; revised 26 October 2024; accepted 29 October 2024. Date of publication 31 October 2024; date of current version 18 November 2024. This work was supported in part by the SGS grant from VSB - Technical University of Ostrava under Grant SP2024/081, in part by European Regional Development Fund—Operational Programme Research, Development and Education, under Grant CZ.02.1.01/0.0/0.0/17\_049/0008425 (Research Platform focused on Industry 4.0 and Robotics in Ostrava agglomeration), and in part by Psychological Research in Selected Areas of Educational and Clinical Psychology IX., under Grant IGA\_FF\_2024\_016. (*Corresponding author: Miroslav Slouka.*)

Miroslav Slouka and Jan Látal are with the Department of Telecommunications, Faculty of Electrical Engineering and Computer Science, VSB-Technical University of Ostrava, 70800 Ostrava, Czech Republic (e-mail: miroslav.slouka.st@vsb.cz).

Ladislav Stanke is with the Department of Psychology, Faculty of Arts, Palacky University Olomouc, 77900 Olomouc, Czech Republic.

Martin Kutáč is with the Department of Homologation and Photometry, Technical Center, HELLA AUTOTECHNIK NOVA, 78985 Mohelnice, Czech Republic.

Digital Object Identifier 10.1109/JPHOT.2024.3489725

might be related to the oxidation processes, cracks, increases in or reductions in the quantum efficiency of the phosphor, etc.

The human eye can detect a color shift when it exceeds the Minimum Perceptible Color Difference (MPCD). This value represents the smallest discernible change in color and is quantified by changes in the chromaticity coordinates ( $u$ ,  $v$ ) [15]. According to study [16], a deviation greater than  $\Delta uv = 0.002$  is unacceptable; thus, this value has been selected as the MPCD to ensure consistent color perception. In addition to color perception, it is important to address that PWM may affect humans in other ways, particularly due to flicker, as discussed in a study [17]. Contrary to common belief, electroretinogram studies show that the human retina can detect modulation frequencies up to 200Hz, even if the flicker is too rapid to be consciously perceived [18]. Non-visual effects of flickering light, such as blood pressure modulation, have also been reported [19]. However, the experimental study presented here does not account for the impact of flicker on human perception or potential health risks associated with the application of PWM. Visible flicker can pose risks, including seizures or neurological symptoms such as headaches or malaise, while invisible flicker may lead to issues like eye strain and headaches [18]. Although the current study focuses on color perception, these non-visual flicker effects should not be overlooked in future research or practical applications of PWM.




The experimental study presented provides two main results. The first compares the photometric and colorimetric properties of three commercially available LEDs. The second result provides insight into the color rendering of the selected LEDs and their impact on human visual perception. This information is useful to experts in various fields, including the biomedical industry, automotive design, and lighting design, as it is not readily available in the datasheets provided by most LED manufacturers. Typically, datasheets contain information on the chromodynamic coordinate shift as a function of the junction temperature and forward current. The main goal of the presented study is to assess the specifics of PWM LED driving and to determine whether it may have substantial consequences on lighting scenarios where color rendering is a crucial parameter for human color perception or for meeting regulatory requirements, such as those imposed in the automotive sector.

## II. MATERIALS AND METHODS

### A. LED Sources Under Test

We selected a suite of OSRAM SYNIOS LEDs that emit light in the red, yellow, and white spectra for our experimental analysis. The specific models chosen for this study were the KR DMLN31.23 [20], KY DMLN31.FY [21], and KW DMLN31.SG [22]. The selected parameters for these LEDs show in Table I. Each LED variant shares the same chip dimensions of  $500 \mu\text{m}$ , highlighting uniformity in their construction. The red KR DMLN31.23 LED, which falls under the InGaAlP ThinFilm category, which functions without a phosphor coating, relies solely on its p-n junction to define its light emission color. The KY DMLN31.FY yellow LED employs ThinGaN technology and is enveloped in a phosphor dispensing structure

TABLE I  
LED PARAMETERS [20], [21], [22];  $\lambda_{DOM}$  - DOMINANT WAVELENGTH,  $CCT$  - CORRELATED COLOR TEMPERATURE,  $I$  - CURRENT,  $T_{MAX}$  - MAXIMUM TEMPERATURE,  $R_{th}$  - THERMAL RESISTANCE, AND  $P_{th}$  STANDS FOR THERMAL POWER

	KR 31.23	KY 31.FY	KW 31.SG
			
parameter			
Bin	HZ-2-Q3	5H-5F-8E	7J-EBXD46-8F
Chip	InGaAlP	InGaN	InGaN
$\lambda_{DOM}$	621 nm	590 nm	-
$CCT$	-	-	6100 K
$I$	5-250 mA	5-200 mA	5-300 mA
$T_{MAX}$	125 °C	125 °C	125 °C
$R_{th}$	30 $\text{KW}^{-1}$	18 $\text{KW}^{-1}$	18 $\text{KW}^{-1}$
$P_{th}$	0.41 W	0.48 W	0.7 W

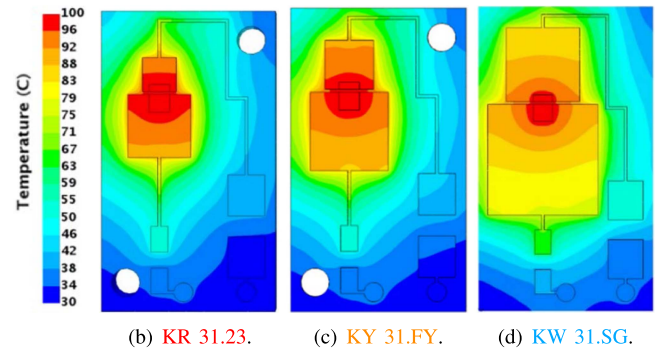


Fig. 1. CFD simulation results of different LED: Displaying the temperature distribution across the test fixture surfaces, these results validate the design of the heat-dissipating surfaces to keep soldering area temperatures at 100 °C.

with a coating encompassing the entire chip housing, refining its spectral output. The KW DMLN31.SG white LED, also using ThinGaN technology, features a targeted phosphor conformal structure where the coating is applied directly to the chip die, ensuring precise color temperature control.

These LEDs were mounted on a glass-reinforced epoxy laminate material (FR4) Printed Circuit Board (PCB) with a standard copper thickness of  $35 \mu\text{m}$ . The Littelfuse FF 250 mA fuses and SS14 1 A 40 V DO-214AC diodes were utilized as protective elements for the LEDs connected in series with the tested LEDs in the circuit.

The geometry of the heat-dissipating surfaces (extended solder pads) was designed to maintain the temperature beneath the LED soldering area of 100 °C under maximum current load. The Computational Fluid Dynamics (CFD) method was employed for calculations, and the results are depicted in Fig. 1, providing a detailed visual representation of the thermal behavior of the test fixtures and reaching the desired temperature in the simulation. These pictures also show how the PCBs were oriented towards the colorimeter during angular measurement. To measure the real temperature and validate the simulated data, a K-type thermocouple (Cr-Al) was soldered to the solder LED pad, ensuring

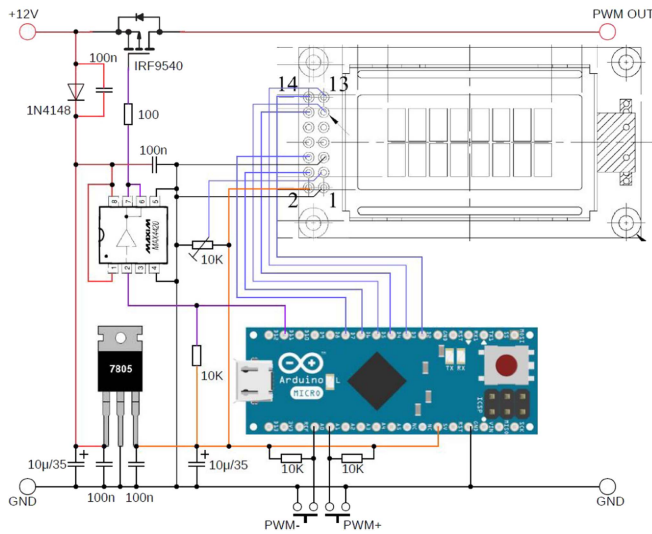


Fig. 2. Schematic diagram of the PWM control circuit.

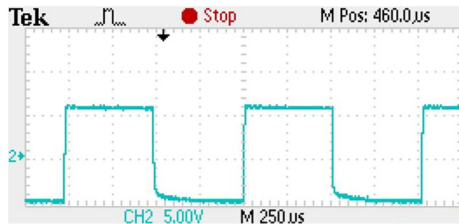


Fig. 3. Oscilloscope trace of a 50% duty cycle PWM voltage signal: The image displays a rectangular waveform.

the CFD predictions' reliability and the LED system's thermal design.

### B. Experimental Setup and Procedure

A dedicated electrical circuit with PWM control was designed for this study to regulate the LED's brightness. This circuit, depicted in Fig. 2, is powered by 12V and steps down to 5V via a 7805 voltage regulator, supplying power to an Arduino Nano, which serves as the central processing unit. User interaction is enabled through PWM+ and PWM- buttons, allowing dynamic adjustment of the PWM duty cycle, visually represented on a display.

The signal processed by the Arduino is driven through a MAX4420 IC to control an IRF9540 Metal Oxide Semiconductor Field Effect Transistor (MOSFET), modulating the current to the LED. Additionally, a current-limiting subcircuit with an LM317 ensures that the LED receives a constant maximum current, as specified in Table I. The switching frequency was set to 1 kHz (1ms period), sufficient for automotive lighting applications. Fig. 3 shows an oscilloscope trace that captures a PWM signal at a 50% duty cycle, displaying the characteristic rectangular waveform of the PWM's on-off pattern.

The experiment involved two different measurement setups to achieve results. The first part aimed to measure the total light output. The scheme, therefore, includes a spherical integrator

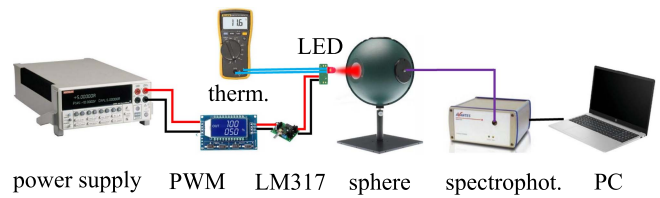


Fig. 4. Schematic for the total light output measurement.

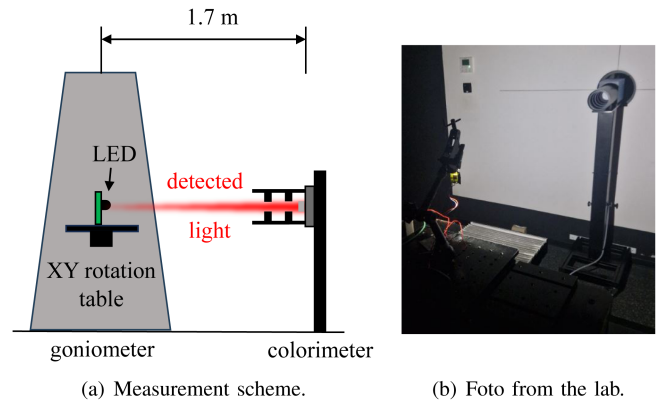


Fig. 5. Goniocolorimetry measurement setup.

AvaSphere-50, and the overall luminous flux and chromaticity coordinates were detected by spectrophotometer AvaSpec-HS2048. The circuit was powered via KEITHLEY 2302, and a thermometer OMEGA CL3512A sensed the temperature. In the case of CW control mode, the PWM circuit has been omitted. The luminous flux measurements were associated with an uncertainty of 3.5% for this assembly according to the calibration data [23]. Spectral measurement uncertainty was quantified as follows:

$$u_b = \frac{1/2 \cdot \text{FWHM}}{\sqrt{3}} = 1.56 \text{ nm}, \quad (1)$$

where the Full Width at Half Maximum (FWHM) is catalog-listed at 5.5 nm, and  $\sqrt{3}$  represents the coefficient associated with a uniform distribution [24]. This is shown in Fig. 4.

The second part of the experiment dealt with angular measurements of color coordinates using a set of LMT1660 goniophotometers with the fast scanning colorimeter LMT C3300 as shown in Fig. 5(a). This is an a Type A goniometer according to IES LM-75-01 [25] with the range of  $V \pm 90^\circ$  (vertically) and  $H \pm 90^\circ$  (horizontally) with the uncertainty of  $0,01^\circ$  for both axes [26]. The colorimeter was 1.7m from the LED to be measured. This device simultaneously acquired and integrally determined X, Y, Z tristimulus values, eliminating measurement errors caused by fluctuations in test object characteristics over time. The resolution is according to the calibration list [27] 0.001 for both x-coordinates and y-coordinates in  $x = 0,4480$  and  $y = 0.4083$ . The detector area is circular with a radius of 5 cm [28]. A photo of the lighting lab measurement is shown in Fig. 5(b). A Jäger MLNG laboratory power supply was used in this setup.

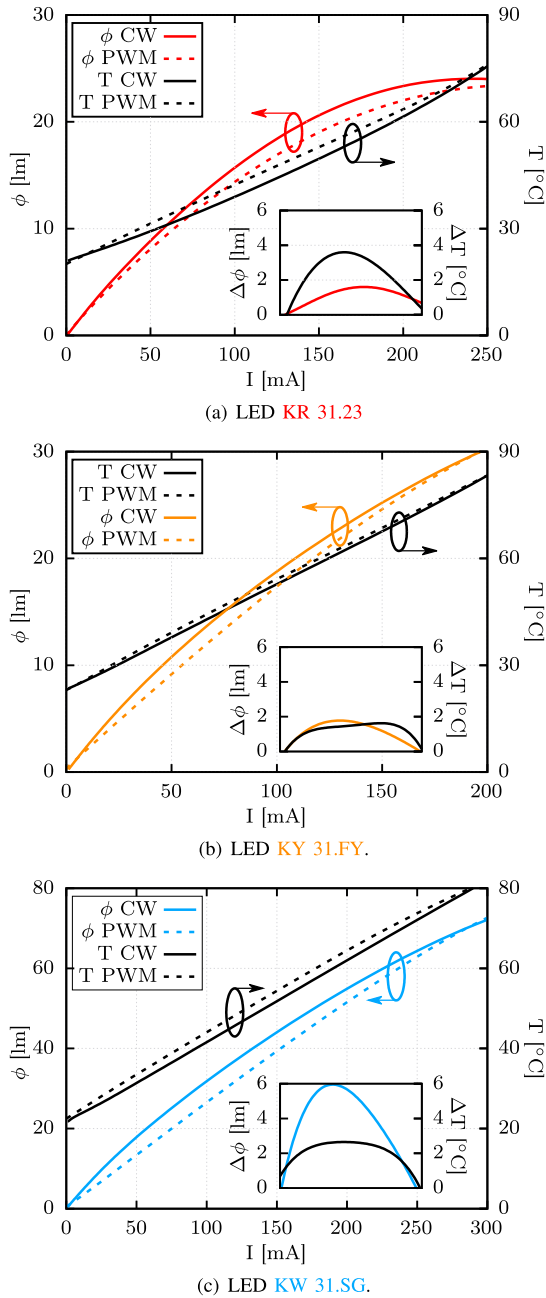


Fig. 6. Comparative analysis of luminous flux ( $\phi$ ) and soldering pad temperature ( $T$ ) against the current ( $I$ ), comparing the performance under CW and PWM mode. The data points are fitted with a Bezier curve.

### III. RESULTS

Figures detailing the results of an experimental study on the performance of OSRAM SYNIOS LEDs are shown in Figs. 6–10. These results illustrate the behavior of these LEDs under two different control methods: CW and PWM modes.

#### A. Light Flux and Temperature

The results in Fig. 6 present a thorough analysis of the luminous flux ( $\phi$ ) and soldering pad temperature ( $T$ ) against the average current ( $I$ ). The differences ( $\Delta$ ) of the displayed curves

TABLE II  
PEAK DIFFERENCES IN LUMINOUS FLUX ( $\Delta\phi$ ) AND SOLDERING PAD TEMPERATURE ( $\Delta T$ ) BETWEEN CW AND PWM MODES: THE SIGN OF  $\Delta$  INDICATES WHETHER THE VALUE IS HIGHER (POSITIVE) OR LOWER (NEGATIVE) IN CW MODE COMPARED TO PWM MODE

LED	$\Delta\phi$ [lm]	$\Delta T$ [°C]
KR 31.23	+1.8 (8.4%)	-4.1 (9.5%)
KY 31.FY	+2.1 (13.3%)	-2.0 (2.9%)
KW 31.SG	+6.6 (19.9%)	-2.7 (6.1%)

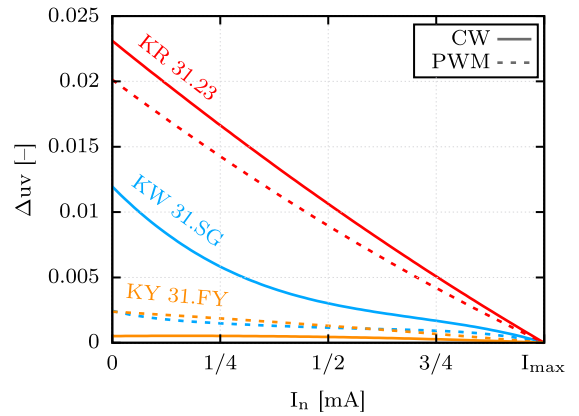


Fig. 7. The  $\Delta uv$  with normalized current  $I_n$  up to  $I_{max}$ . Bezier fit was used.

between CW and PWM modes are shown in the inset graphs. In CW control mode, the temperature is maintained at a lower level, allowing for a higher luminous flux, suggesting a more efficient operation in luminous output than in PWM mode. This indicates that CW control mode is beneficial from the standpoint of luminous efficacy. On the other hand, when PWM control is employed, there is a noticeable increase in temperature and a reduction in average luminous flux for the same average current level, which may imply a less efficient operation. The LED in PWM mode heats more because the instantaneous power value is higher here than in CW mode. There is always a constant value of instantaneous voltage and current with PWM; only the time for which this power is delivered changes.

The Table II shows the comparative analysis of luminous flux and soldering pad temperature variances between modes. The red LED exhibits a luminous flux change of 1.8lm, an 8.4% difference, and a temperature shift of 4.1 °C, a 9.5% variance when comparing CW to PWM modes. The yellow LED shows a slightly higher flux change at 2.1 lumens (13.3%) and a more minor temperature change of 2 °C (2.9%). The white LED presents the most substantial flux change at 6.6 lumens (19.9%) and a temperature difference of 2.7 °C (6.1%). These figures indicate that the control mode significantly affects LEDs' power and thermal performance.

#### B. Total Color-Shift

The color shift in total light output with increasing current in both modes is shown in Fig. 8. Corresponding  $\Delta uv$  shows Fig. 7 where the  $\Delta uv$  is calculated as the Euclidean distance between the current and reference data point at  $I_{max}$ .

TABLE III  
 $\Delta uv$  IN TOTAL LIGHT OUTPUT

LED	CW [-]	PWM [-]	$\Delta$ [-]
KR 31.23	0.0231	0.0201	+0.003
KY 31.FY	0.0005	0.0024	-0.0019
KW 31.SG	0.019	0.0024	+0.0095

The Euclidean distance between the data point at  $I_{MIN}$  and  $I_{MAX}$ : the sign of  $\Delta$  indicates whether the value is higher (positive) or lower (negative) in CW mode compared to PWM mode.

The figures are presented in the CIE 1931 color space [29], with marked areas indicating compliance with ECE R148 [30] and nominal CCT categories according to ANSI C78.377-2017 [31]. The LED KR 31.23 exhibits a significant color shift in both CW and PWM modes and has the highest  $\Delta uv$  values, confirming this statement. The difference between CW and PWM modes is minimal, with the maximum difference around  $\Delta uv = 0.003$  at minimum current, showing a linear trend as the current increases. For LED KY 31.FY, the color shift is only slight, with the PWM mode showing a more pronounced shift than the CW. It shows the lowest  $\Delta uv$  values. The difference between CW and PWM modes for KY 31.FY is also minimal, with a maximum difference of  $\Delta uv = 0.0019$  at minimum current, following a linear trend with increasing current. The LED KW 31.SG exhibits a significant color shift in CW mode, but the chromaticity remains within the 5700K CCT ANSI range even with this notable color shift. In contrast, in PWM mode, the color remains significantly more stable with changes in current.  $\Delta uv$  values confirm the following statements, but the difference between the CW and PWM modes for KW 31.SG is significant, with nearly a  $\Delta uv = 0.01$  at the minimum current, which decreases exponentially as the current increases. These trends are summarized in Table III.

### C. Angular Color-Shift

Angular color shifts in CIE 1931 are shown with an increasing horizontal angle from  $0^\circ$  to  $80^\circ$  with  $5^\circ$  step in the CW and PWM modes in Fig. 9 and  $\Delta uv$  in Fig. 10. The LED KR 31.23 shows a minimal angular color shift up to  $60^\circ$ , then changes manifest, especially at low currents, reaching approximately  $\Delta uv = 0.01$  for CW and  $\Delta uv = 0.006$  for PWM. All points are on the edge of the trichromatic diagram, showing that changing the angle does not affect the chromaticity of the LED. For LED KY 31.FY CW 20 and 200mA hardly change color with angle,  $\Delta uv$  displays a moderate increase with an angle that peaks at 0.002. However, at a PWM of 20mA, a shift at angles above  $70^\circ$  reached  $\Delta uv = 0.6$  at  $80^\circ$ . LED KW 31.SG exhibits notable shifts in chromaticity within the ANSI CCT area. The CW is from 6500K over 5700K areas to protruding from the chromatic region at angles above  $70^\circ$ . For PWM at 20 mA, there is a shift of the total shifter range, which starts in the 5700K region and leaves at an angle of  $50^\circ$ . The shift continues longer in the yellow area of the trichromatic diagram and at an angle of  $60^\circ$ , the light output becomes illegal regarding ECE R148 regulation. The  $\Delta uv$  curves exhibit similar trends for both CW and PWM

modes. They consistently increase, reaching a maximum value close to  $\Delta uv = 0.03$  at  $80^\circ$ .

## IV. DISCUSSION AND STUDY LIMITATION

To analyze driving current influence on optical and visual performance, three typical automotive LEDs were chosen for experimental testing. These were red KR 31.23, yellow KY31.FY and white phosphor-converted KW 31.SG. Firstly the light flux and solder pad temperatures were measured. With the CW drive current, all tested LEDs achieved higher flux levels and lower solder pad temperatures. Most significant changes were observed with the white 31.SG LED illustrates how important the driving current tuning is, especially for the white color functions, while reaching an almost 20% increase in the luminous flux and 6.1% lower temperature. The red KR31.23 LED achieved almost 10% increase in soldering pad temperature and the yellow KY 31.FY achieved the least significant temperature increase reaching almost 3% while using PWM mode. Both luminous flux values were increased similarly in the case of red and yellow LEDs, which gave approximately 2 more lumens while employing CW mode. Luminous flux differences between the CW and PWM driving modes are typically maximal in the middle of the current range while blurred around the lowest and highest values. The temperature difference trends among the chosen LEDs are less similar. Hence, the lighting designer or engineer should choose the appropriate driving current mode based on the cost-benefit analysis, which assesses the luminous flux and temperature increase for a specific current level while considering the thermal design of the whole system.

From the visual performance point of view, PWM driving might provide with important advantage, especially for white PC LEDs. If a single type of white PC LEDs should provide several illumination levels, the PWM can provide a dimming option with a minimized color difference across several dimming states. This can be useful, for instance, if the same LEDs provide parking or position functions together with daytime running lamps. The difference between CW and PWM drive is significant, in comparison with red or yellow LED, in which case the CW is, unlike the previous two, providing with lower color difference while dimming is applied. Hence, this advantage diminishes for color LEDs.

It was also shown that for both red and yellow LED, the light output remains within the boundaries of ECE red and yellow, respectively, as defined within the ECE R148 regulation. This is also true for the white LED, for which the light output is also within the ECE-defined region. It can be seen that with the PWM, it is easier to remain within the nominal CCT quadrangle, which corresponds to the statement from the previous paragraph. With the PWM driving, the light output tends to have a higher CCT, whereas with CW, the light covers a broader CCT range and achieves much lower CCT than with the PWM driving mode, especially for lower current values.

Another important aspect that is less often assessed in this level of detail is the color constancy of LEDs not only when different drive current modes are selected but also when perceived

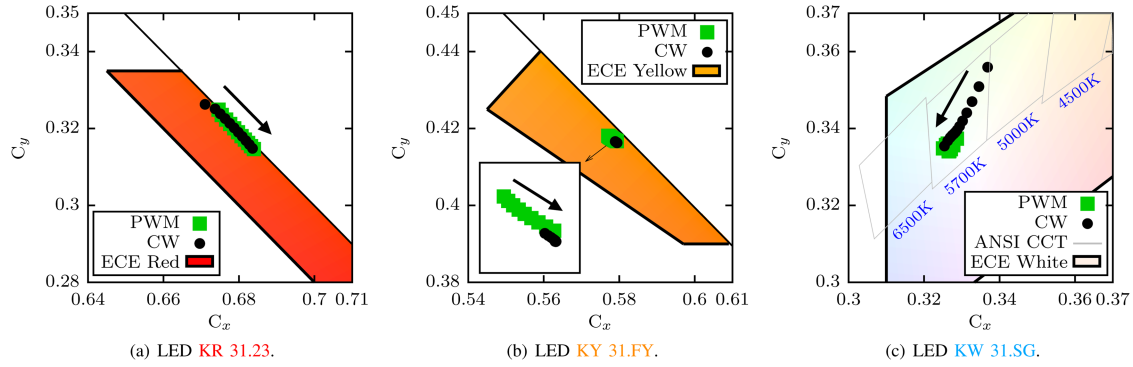


Fig. 8. Color-shift in the total light output with increasing current of 1mA to  $I_{max}$  with 25mA step in CW and PWM mode. The view is in the CIE 1931 color space [29] with marked areas indicating compliance with ECE Regulation No. R148 [30] and nominal CCT categories with ANSI C78.377-2017 [31]. Data were obtained using a spectrophotometer. The arrow shows the direction of increasing current.

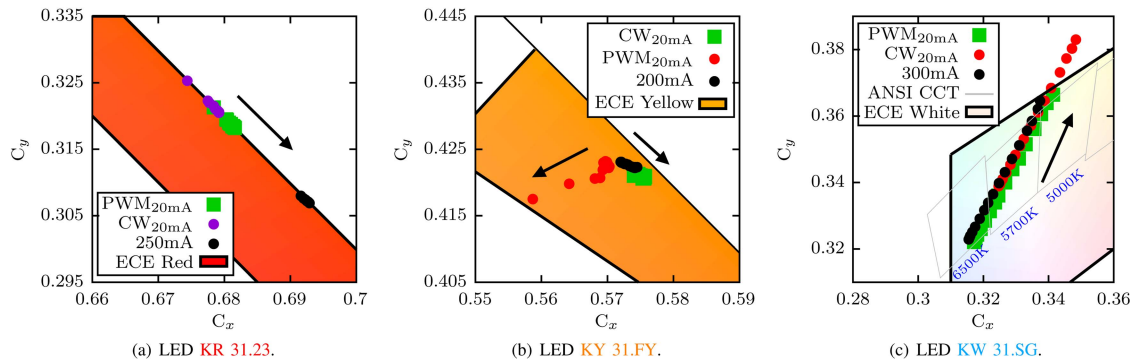


Fig. 9. Angular color-shift with increasing horizontal angle from  $0^\circ$  to  $80^\circ$  with  $5^\circ$  step in CW and PWM modes. The view is again in the CIE 1931 color space [29] with marked areas indicating compliance with ECE Regulation No. R148 [30] and nominal CCT categories with ANSI C78.377-2017 [31]. Data were obtained using a goniochromimeter. The arrow shows the direction of increasing angle.

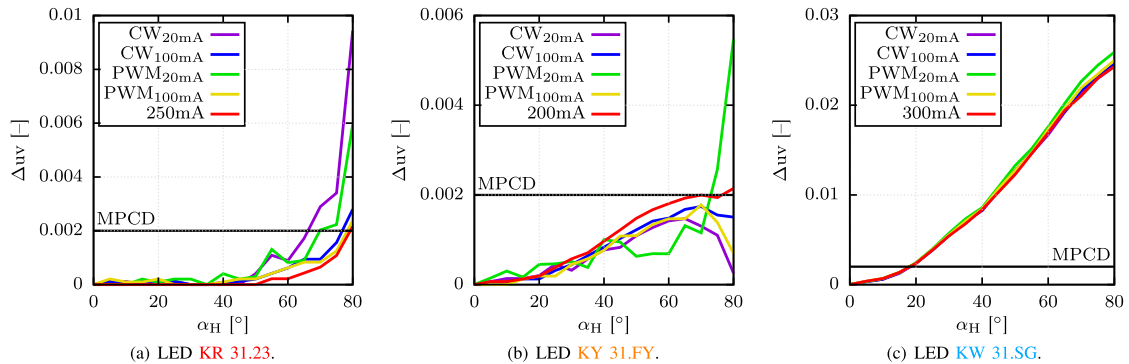


Fig. 10. Angular  $\Delta uv$  with increasing horizontal angle from ( $\alpha_H$ ) from  $0^\circ$  to  $80^\circ$  with  $5^\circ$  step in CW and PWM modes. The  $\Delta uv$  is calculated as the Euclidean distance between the current and reference data point at  $0^\circ$ . The selected currents are 20mA, 100mA, and  $I_{max}$ . The MPCD value is marked.

from different observing angles or even in their combination. Hence, angular color uniformity (ACU) was assessed for both driving modes. ACU was assessed as it also possesses the possible consequences on the legality of light sources from the perspective of regulatory bodies. To assess conformity, we used the boundaries for red, yellow, and white colors as defined in the ECE regulations, while to assess consistency of color, we

applied MPCD based on the color distance of  $\Delta uv > 0.002$ . This threshold is rather strict and allows testing whether the LEDs can be applied in high-performance use cases requiring precisely maintained color rendering. The ACU analysis showed that the red LED ACU is better achieved with PWM than with low-current CW. The difference between CW and PWM for high current values becomes less significant. Low-current CW

operation for the white PC LED also leads to the highest risk of producing white light that does not conform to the ECE regulations. This might be an issue when the light is collected from a broader part of the beam. For the yellow LED, the PWM driving mode is less appropriate from the regulatory point of view, where with the increasing angle, the light output is close to the ECE Yellow borderline. Regarding ACU, our results indicate that for maximum angular deviations, the  $\Delta\text{CCT}$  values for the white PC LED are greater than those achieved with LEDs using specific methods to mitigate ACU, such as those described in [12]. In this study, the light emitted from the white LED spans three adjacent nominal CCT quadrants. It extends beyond the ECE-defined boundaries for white color, indicating a substantial color shift. ACU presents less of a challenge for the red and yellow LEDs; however, ACU is notably lower for the yellow LED under PWM control than CW mode. These findings suggest that, particularly for white PC LEDs, it would be advantageous for potential LED users to access an MPCD-based viewing angle in LED datasheets, as this angle is significantly narrower than the conventional 50% intensity viewing angle. For the white LED used in this study, an MPCD-based viewing angle with a threshold of  $\Delta uv > 0.002$  would be approximately one-third of the standard viewing angle at half of the maximum intensity.

The main limitation is that the results represent only the behavior of 3 specifically selected and commercially available LEDs. However, these were carefully chosen to represent examples of LEDs applicable to main and signal headlamp and rear lamp functions. In these applications, the ability to maintain constant color rendering is of crucial importance, mainly due to regulatory requirements. Nevertheless, it is also important for high-quality color rendering, leading to the best visual perception and aesthetic requirements especially when combining LEDs with plastic optical components and other optical components that are prone to chromatic aberrations. Those components might additionally cause further color shifts. In that matter, the provided information might also be purposeful for developers to precompensate chromaticity coordinate shifts induced mainly by the absorption in plastic optical components (e.g., light guides) with the readily available PWM driving circuits together with the fine-tuning of their electrical current parameters and thermal management of the applied setup.

Another limitation of the presented paper is that it does not provide any information about the resulting LED flicker or its influence on the observer's visual performance, as this was not the main goal of this paper. Prospective LED users should conduct their flicker measurements to achieve the desired results with the PWM driving circuitry that assures the desired safety and the observer's visual comfort. It needs to be stressed that the visual and non-visual effects that might arise from the PWM application leading to LEDs' flicker were not studied in the presented article.

## V. CONCLUSION

This study presents a methodology for assessing LEDs' optical and visual performance in automotive applications. The focus is on meeting regulatory requirements and

ensuring consistent color perception together with heat dissipation and energy efficiency. These requirements are growing, especially in electric vehicles. These results provide valuable insight into optimizing current control to maintain these specific requirements.

In tests on three automotive LEDs, differences in luminous flux, thermal behavior, and color shift were observed between CW and PWM control. Under PWM control, all LEDs tested exhibited lower luminous flux and higher heat sink temperatures. For red non-luminophore InGaAlP LEDs, there were no significant color differences between the CW and PWM control. CW control was more advantageous in yellow InGaN LEDs with a dispensing phosphor structure, providing better resistance to total and angular color shifts. From the perspective of color stability, PWM control proved beneficial for white InGaN LEDs with a conformal phosphor layer, where it improved color stability and allowed compliance with color output requirements even at wide viewing angles.

The choice between PWM and CW control should always consider the application's specific requirements, including regulatory standards, safety, thermal management, and visual properties. This study's findings indicate that PWM control is suitable for color stabilization in white LEDs, while CW control is better suited to applications where optical performance is prioritized. The study also recommends including MPCD-based viewing angles in datasheets for high-precision applications, providing valuable information for optical engineers and designers when optimizing LED performance.

## REFERENCES

- [1] S. Winder, *Power Supplies for LED Driving*. London, U.K.: Newnes, 2011.
- [2] P. Padmavathi and S. Natarajan, "A survey on efficient converter driver techniques for LED LIGHTING applications," in *Proc. Innov. Power Adv. Comput. Technol.*, 2019, pp. 1–7.
- [3] M. W. Umar, N. B. Yahaya, and Z. B. Baharuddin, "PWM dimming control for high brightness LED based automotive lighting applications," *Int. J. Elect. Comput. Eng.*, vol. 7, no. 5, pp. 2434–2440, 2017.
- [4] M. Slouka, L. Folta, L. Stanke, J. Latal, and P. Siska, "Laser diode PWM control and its consequences on optical characteristics," *IEEE Access*, vol. 11, pp. 66777–66792, 2023, doi: [10.1109/ACCESS.2023.3288538](https://doi.org/10.1109/ACCESS.2023.3288538).
- [5] Y. Gu, N. Narendran, T. Dong, and H. Wu, "Spectral and luminous efficacy change of high-power LEDs under different dimming methods," *Proc. SPIE*, vol. 6337, 2006, Art. no. 63370J, doi: [10.1117/12.679907](https://doi.org/10.1117/12.679907).
- [6] H. Chen, S.-C. Tan, S. Yuen, and R. Hui, "Color variation reduction of GaN-based white light-emitting diodes via peak-wavelength stabilization," *IEEE Trans. Power Electron.*, vol. 29, no. 7, pp. 3709–3719, Jul. 2014, doi: [10.1109/TPEL.2013.2281812](https://doi.org/10.1109/TPEL.2013.2281812).
- [7] S. Chhajed, Y. Xi, Y.-L. Li, T. Gessmann, and E. F. Schubert, "Influence of junction temperature on chromaticity and color-rendering properties of trichromatic white-light sources based on LEDs," *J. Appl. Phys.*, vol. 97, no. 5, 2005, Art. no. 054506, doi: [10.1063/1.1852073](https://doi.org/10.1063/1.1852073).
- [8] V. Kumar, A. Sinha, and U. Farooque, "Concentration and temperature dependence of the energy gap in some binary and alloy semiconductors," *Infrared Phys. Technol.*, vol. 69, pp. 222–227, 2015, doi: [10.1016/j.infrared.2015.02.002](https://doi.org/10.1016/j.infrared.2015.02.002).
- [9] M. Leroux et al., "Quantum confined stark effect due to built-in internal polarization fields in (Al,Ga)N/GaN quantum wells," *Phys. Rev. B*, vol. 58, no. 20, pp. R13371–R13374, 1998.
- [10] C. M. Tan, P. Singh, W. Zhao, and H. C. Kuo, "Physical limitations of phosphor layer thickness and concentration for white LEDs," *Sci. Rep.*, vol. 8, 2018, Art. no. 2452, doi: [10.1038/s41598-018-20883-3](https://doi.org/10.1038/s41598-018-20883-3).
- [11] J. P. You, N. T. Tran, Y. C. Lin, Y. He, and F. G. Shi, "Phosphor-concentration-dependent characteristics of white LEDs in different current regulation modes," *J. Electron. Mater.*, vol. 38, no. 6, pp. 761–766, 2009, doi: [10.1007/s11664-009-0754-y](https://doi.org/10.1007/s11664-009-0754-y).

- [12] C. C. Sun et al., "High uniformity in angular correlated-color-temperature distribution of white LEDs from 2800K to 6500K," *Opt. Exp.*, vol. 20, no. 6, pp. 6622–6630, 2012, doi: [10.1364/OE.20.006622](https://doi.org/10.1364/OE.20.006622).
- [13] S. Wang, X. Chen, M. Chen, H. Zheng, H. Yang, and S. Liu, "Improvement in angular color uniformity of white light-emitting diodes using screen-printed multilayer phosphor-in-glass," *Appl. Opt.*, vol. 53, no. 36, pp. 8492–8498, 2014, doi: [10.1364/AO.53.008492](https://doi.org/10.1364/AO.53.008492).
- [14] J. L. Davis et al., "Understanding and controlling chromaticity shift in LED devices," in *Proc. 18th Int. Conf. Thermal Mech. Multi-Phys. Simul. Exp. Microelectronics Microsystems*, 2017, pp. 1–8, doi: [10.1109/EuroSimE.2017.7926223](https://doi.org/10.1109/EuroSimE.2017.7926223).
- [15] Commission Internationale de L'Éclairage, *CIE 1960 Uniform Chromaticity Scale (UCS) Diagram*, CIE Standard 17-23-079, 1960. [Online]. Available: <https://cie.co.at/eilvterm/17-23-079>
- [16] S. Muthu, F. J. P. Schuurmans, and M. D. Pashley, "Red, green and blue LED based white light generation: Issues and control," in *Proc. 37th Ind. Appl. Conf.*, 2002, pp. 327–333.
- [17] B. Lehman and J. A. Wilkins, "Designing to mitigate effects of flicker in LED lighting: Reducing risks to health and safety," *IEEE Power Electron. Mag.*, vol. 1, no. 3, pp. 18–26, Sep. 2014, doi: [10.1109/MPEL.2014.2330442](https://doi.org/10.1109/MPEL.2014.2330442).
- [18] J. A. Wilkins, J. A. Veitch, and B. Lehman, "LED lighting flicker and potential health concerns: IEEE standard PAR1789 update," in *Proc. 2010 IEEE Energy Convers. Congr. Expo.*, 2010, pp. 171–178, doi: [10.1109/ECCE.2010.5618050](https://doi.org/10.1109/ECCE.2010.5618050).
- [19] L. Tang, X. Zhang, X. Zhou, X. Gu, S. Fan, and M. Liu, "Study of heart rate and blood pressure subject to pulsed LED lighting," *Leukos*, vol. 18, pp. 145–153, 2021, doi: [10.1080/15502724.2021.1920974](https://doi.org/10.1080/15502724.2021.1920974).
- [20] OSRAM, "Datasheet SYNIOS P2720 KY DMLN31.23 Version 1.7," *OSRAM Opto Semiconductors*, Feb. 18, 2021. [Online]. Available: [www.osram-os.com](http://www.osram-os.com)
- [21] OSRAM, "Datasheet SYNIOS P2720 KY DMLN31.FY Version 1.6," *OSRAM Opto Semiconductors*, May 11, 2021. [Online]. Available: [www.osram-os.com](http://www.osram-os.com)
- [22] OSRAM, "Datasheet SYNIOS P2720 KW DMLN31.SG Version 1.7," *OSRAM Opto Semiconductors*, Feb. 18, 2021. [Online]. Available: [www.osram-os.com](http://www.osram-os.com)
- [23] Calibration Certificate: Irradiance Calibration Report for AvaSpec-ULS2048XL-USB2, "Calibration performed with UV transfer standard from LOT Quantum Design GmbH and VIS/NIR transfer standard from NIST, traceable to NIST standards. Test No: 685/289682-17, Version 1.0," Feb. 14, 2022.
- [24] Avantes, "AvaSpec-HS2048XL-EVO SensLine high UV and NIR sensitivity back-thinned CCD spectrometer," Datasheet AVANTES, Jul. 2020
- [25] Illuminating Engineering Society, *Approved Method: Guide to Goniometer Measurements and Types, and Photometric Coordinate Systems*, IES Standard ANSI/IES LM-75-19, New York, NY, USA, 2019.
- [26] LMT Lichtmesstechnik GmbH, "Goniophotometer LMT GO-H 1600," Datasheet, Berlin, Germany. [Online]. Available: <https://lmt.de/index.html?p=373.html>
- [27] LMT Lichtmesstechnik GmbH, "Calibration certificate of the goniophotometer LMT 1660," Berlin, Germany, 2019.
- [28] LMT Lichtmesstechnik GmbH, "Tristimulus colorimeter LMT C. 3300," Datasheet, Berlin, Germany. [Online]. Available: <https://www.lmt.de/tristimulus-colorimeter-lmt-c-3300/>
- [29] CIE, *CIE 1931 Colour-Matching Functions, 2 degree observer (datatable)*, International Commission on Illumination (CIE), Vienna, Austria, 2018, doi: [10.25039/CIE.DS.xvudnb9b](https://doi.org/10.25039/CIE.DS.xvudnb9b).
- [30] United Nations Economic Commission for Europe, "UN regulation no 148 - Light signalling devices (LSD)," 2021.
- [31] American National Standards Institute, *American National Standard for Electric Lamps—Specifications for the Chromaticity of Solid State Lighting (SSL) Products*, ANSI C78.377-2017 (R2022), 2023.